# *Zitterbewegung* of Moiré Excitons in Twisted $MoS_2/WSe_2$ Heterobilayers

I. R. Lavor,[1,2,3] D. R. da Costa,[1] L. Covaci,[3] M. V. Milošević,[3] F. M. Peeters,[3] and A. Chaves[1,3]
[1]*Departamento de Física, Universidade Federal do Ceará, 60455-760 Fortaleza, Ceará, Brazil*
[2]*Instituto Federal de Educação, Ciência e Tecnologia do Maranhão, KM-04, Enseada, 65200-000 Pinheiro, Maranhão, Brazil*
[3]*Department of Physics, University of Antwerp, Groenenborgerlaan 171, B-2020 Antwerp, Belgium*

(Received 11 February 2021; accepted 28 June 2021; published 31 August 2021)

The moiré pattern observed in stacked noncommensurate crystal lattices, such as heterobilayers of transition metal dichalcogenides, produces a periodic modulation of their band gap. Excitons subjected to this potential landscape exhibit a band structure that gives rise to a quasiparticle dubbed the moiré exciton. In the case of $MoS_2/WSe_2$ heterobilayers, the moiré trapping potential has honeycomb symmetry and, consequently, the moiré exciton band structure is the same as that of a Dirac-Weyl fermion, whose mass can be further tuned down to zero with a perpendicularly applied field. Here we show that, analogously to other Dirac-like particles, the moiré exciton exhibits a trembling motion, also known as *Zitterbewegung*, whose long timescales are compatible with current experimental techniques for exciton dynamics. This promotes the study of the dynamics of moiré excitons in van der Waals heterostructures as an advantageous solid-state platform to probe *Zitterbewegung*, broadly tunable by gating and interlayer twist angle.

DOI: 10.1103/PhysRevLett.127.106801

*Introduction.—Zitterbewegung* (ZBW) is a fast trembling motion of elementary particles that obey the Dirac equation [1], predicted by Schrödinger in 1930 for relativistic fermions [2]. Schrödinger observed that the components of the relativistic velocity for particles in vacuum does not commute with the free-particle Hamiltonian [2]. As a consequence, the expectation value of the position operator for a fermion wave packet displays rapid oscillatory motion, owing to the fact that the velocity is not a constant of motion, as well as to the interference between the positive and negative energy states composing the wave packet [2–4].

Since the Dirac equation predicts ZBW with amplitude of the order of the Compton wavelength ($10^{-2}$ Å) and a frequency of $\omega_{ZB} \approx 10^{21}$ Hz, which are not accessible with current experimental techniques [5], a direct experimental observation of this effect is challenging. Therefore, the past decades have seen an increasing interest in the ZBW phenomena in different systems, such as ultracold atoms [6,7], semiconductors [8–13], carbon nanotubes [14], topological insulators [15], crystalline solids [16,17], and other systems [18–22]. In fact, ZBW has been experimentally detected using quantum simulations of the Dirac equation based on trapped ions [22], Bose-Einstein condensates [24,25], and, most recently, an optical simulation [26]. Since the characteristic frequency of ZBW is determined by the energy gap between the (pseudo)spin states [9], designing a system where the gap in the Dirac cone can be controlled at will is fundamental for optimization of the oscillation frequency and eventual experimental detection of this phenomenon.

Most recently, advances in the isolation of monolayer semiconductors and their stacking as van der Waals heterostructures (vdWHSs) opened a new field of study of artificial 2D hybrid materials [27,28]. Combining two monolayers of semiconducting transition metal dichalcogenides (TMDs) in a vdWHS with an interlayer twist introduces an in plane moiré pattern [29], as illustrated in Fig. 1(a). This pattern is associated with an in plane modulation of the conduction and valence band edges, thus presenting new possibilities to engineer the electronic band structure, quasiparticle confinement, and optical properties of the system. Especially, interlayer excitons (ILEs) are profoundly affected by the moiré pattern, which creates regions in space where the ILE energy is significantly lower. For $MoS_2/WSe_2$ vdWHS with small twist angle ($R$-type stacking) [30], lowest energy regions are those with stacking registry $R_h^h$ and $R_h^X$, represented by $A$ and $B$ in Fig. 1(a). These regions form a honeycomb superlattice for excitonic confinement, thus leading to a moiré exciton band structure that resembles the one of gapped monolayer graphene. Different interlayer distances for $R_h^h$ and $R_h^X$, as illustrated in Fig. 1(b), lead to different ILE dipole moments in each region. Consequently, a perpendicularly applied electric field $\varepsilon$ can be used to tune the energies of $A$ and $B$ ILE sublattices, thus making them equal at $\varepsilon = \varepsilon_0 \approx 0.44$ V/nm [31]. In this case, the moiré exciton band structure acquires a massless Dirac fermion character, as illustrated in Fig. 1(c). The combination of the long lifetime and bright luminescence [31] of ILEs, along with their Dirac-like dispersion tunable by the twist angle and applied fields, makes twisted vdWHS a strong candidate for experimental detection of ZBW of moiré excitons.

In this Letter, we analyze the dynamics of moiré exciton wave packets as an optoelectronics-based platform to probe

 

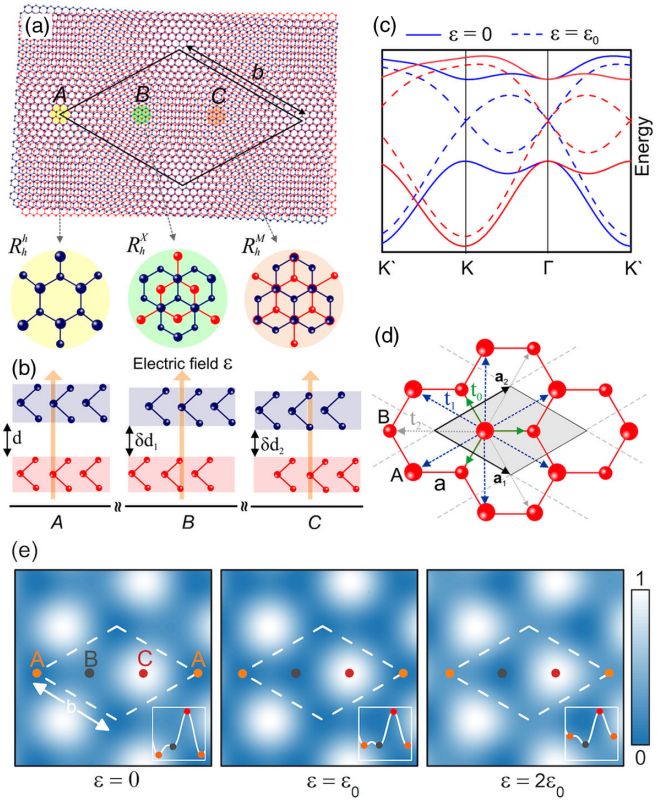


FIG. 1. (a) Moiré pattern with period $b$ in an $MoS_2/WSe_2$ heterobilayer, twisted by 3°. Black diamond represents the supercell. Insets magnify three characteristic locations ($A$, $B$, and $C$), where atomic registries resemble lattice-matched bilayers of different $R$-type stacking. (b) Lateral view of the interlayer distance of the regions $A$, $B$, and $C$ (for more details, see Ref. [31]). (c) Corresponding band structures, calculated with the tight-binding model, for the first moiré Brillouin zone with (dashed lines) and without (solid lines) an applied electric field ($\varepsilon = \varepsilon_0 \approx 0.44$ V/nm) for the $K$ (red) and $K'$ (blue) valleys of the crystal. (d) Representation of a honeycomb lattice structure and unit cell (gray region) where sublattice sites $A$ and $B$ correspond to the respective stacking registries labeled in (a) and with lattice constant $a$. First, second, and third nearest-neighbors hopping parameters are represented by $t_0$ (green arrows), $t_1$ (blue arrows), and $t_2$ (gray arrows), respectively. $\vec{a}_1$ and $\vec{a}_2$ are the basis vectors. (e) Color map of the ILE potential landscape in $R$-type $MoS_2/WSe_2$, as illustrated in (a), where the excitonic potential is tuned by an applied perpendicular electric field $\varepsilon$. The inset in each panel shows the potential profile along the high-symmetry points ($A - B - C - A$) of the moiré supercell. For $\varepsilon = \varepsilon_0$, the excitonic potential exhibits the same value at regions $A$ and $B$, whereas for $\varepsilon = 2\varepsilon_0$ ($\varepsilon = 0$), $A$ ($B$) becomes higher in energy than $B$ ($A$).

ZBW, as an alternative to the previous proposals, mostly based on low-energy electrons in graphene or on ultracold atoms. To do so, we apply the time-evolution operator [32,33] on a wave packet distribution representing a moiré exciton in twisted $MoS_2/WSe_2$ vdWHSs. We discuss the effects of the wave packet parameters, such as its pseudospinor and width, as well as of an applied electric field and different twist angles, on the ZBW amplitude and time evolution of the exciton probability density distribution. The optimization of parameters proposed here may guide future experiments toward the experimental observation of ZBW of such neutral quasiparticles in this vdWHS, which represents an important advance in the understanding not only of this phenomenon, but also of the tunable Dirac-like character of the moiré exciton.

*Tight-binding approach for excitons in a potential landscape.*—ILEs in a twisted heterobilayer experience a periodic potential of the form [31]

$$V(\vec{r}) = E_g[\vec{r}_0(\vec{r})] + e\varepsilon d[\vec{r}_0(\vec{r})] - E_b, \tag{1}$$

where $d$ is the interlayer distance and $E_g$ the ILE band gap [34], both modulated along the plane due to the moiré pattern (see Fig. 1), and $\varepsilon$ is a perpendicularly applied electric field. Here, $\vec{r}_0$ is the in plane displacement vector from a metal site in the hole layer to a nearest-neighbor metal site in the electron layer, depending on the location $\vec{r}$ in the moiré pattern. The binding energy $E_b$, on the other hand, is not expected to be significantly dependent on the local potentials [31] and is, therefore, assumed to be constant.

Excitons in such a potential landscape would be trapped at their local minima and exhibit a nonzero (complex) hopping to the neighboring minima. In a twisted $MoS_2/WSe_2$ bilayer, this landscape of energy minima has a honeycomb symmetry, with $A$ ($R_h^h$) and $B$ ($R_h^X$) sublattices at slightly different energies, $+\delta$ and $-\delta$, respectively. A low-energy quasiparticle—in this case, an exciton—in such a landscape would behave as a nonzero mass Dirac-Weyl fermion, whose Hamiltonian, within third-nearest-neighbors approach, reads [31,35]

$$H_{\text{mex}} = \begin{pmatrix} \delta - t_A F(\vec{k}) & t_0 Z_0(\vec{k}) + t_2 Z_2(\vec{k}) \\ t_0 Z_0^*(\vec{k}) + t_2 Z_2^*(\vec{k}) & -\delta - t_B F(\vec{k}) \end{pmatrix}, \tag{2}$$

where $t_{A(B)}$ is the hopping between nearest-neighbors minima of the $A$ and $B$ sublattices [36] that compose the honeycomb moiré potential, $t_0$ and $t_2$ are hopping parameters between first and third nearest neighbors, see Fig. 1(d), and structure factors are given by

$$\begin{aligned} F(\vec{k}) &= 2\cos[\vec{k}\cdot(\vec{a}_1 - \vec{a}_2) - \theta_s] \\ &\quad + 2[\cos(\vec{k}\cdot\vec{a}_1 + \theta_s) + \cos(\vec{k}\cdot\vec{a}_2 - \theta_s)], \\ Z_0(\vec{k}) &= 1 + e^{-i(\vec{k}\cdot\vec{a}_1 + \theta_s)} + e^{-i(\vec{k}\cdot\vec{a}_2 - \theta_s)}, \\ Z_2(\vec{k}) &= e^{-i\vec{k}\cdot(\vec{a}_1 + \vec{a}_2)} + 2\cos[\vec{k}\cdot(\vec{a}_1 - \vec{a}_2) + \theta_s], \end{aligned}$$

where $\theta_s = 4\pi s/3$ originates from the complex part of the hopping parameters of the moiré exciton [31] with spin sign $s = \pm 1$.

Diagonalization of $H_{\mathrm{mex}}$ leads to the moiré exciton band structure

$$E_{\pm} = -t_{+}F(\vec{k}) \pm \sqrt{|t_0 Z_0(\vec{k}) + t_2 Z_2(\vec{k})|^2 + (t_{-}F(\vec{k}) - \delta)^2}, \tag{3}$$

where $t_{\pm} = (t_A \pm t_B)/2$. An example of such a band structure is shown in Fig. 1(c). In the absence of external field, since the energies of sublattices $A$ and $B$ are different [see left panel in Fig. 1(e)], $\delta \neq 0$ and the moiré exciton band structure exhibits a gap, as illustrated by solid lines in Fig. 1(c). However, as the applied field $\varepsilon$ increases, the sublattices become similar in energy and $\delta$ approaches zero as the field reaches a critical value $\varepsilon_0$, which is 0.44 V/nm for the vdWHSs considered here [see middle panel in Fig. 1(e)]. In this case, the dashed lines in Fig. 1(c) exhibit a gapless Dirac-like band structure for the moiré exciton in the vicinity of the Γ point of the moiré Brillouin zone, which corresponds to either the $K$ or $K'$ points of the crystal Brillouin zone. Different colors in Fig. 1(c) stand for the excitonic band structures of the two possible exciton spins, up or down for $s = +$(red) or $s = -$(blue), respectively. Because of the spin-valley locking, the spin-valley index $s$ also corresponds to a moiré exciton at the $K$ ($K'$) valley for $s = +(-)$ in the considered case of $R$-type stacking registry. As we will consider only large moiré exciton wave packets centered at Γ, where the bands for the two different spins are similar, spins are not expected to play a significant role in this study.

*Wave packet dynamics.*—Writing the Hamiltonian as $H = \vec{\alpha}\cdot\vec{\sigma}$, where $\vec{\sigma}$ are the Pauli matrices, allows one to easily apply the time-evolution operator in an exact form as a simple matrix multiplication [32,33,37]. Therefore, it is convenient to rewrite Eq. (2) as

$$H_{\mathrm{mex}} = \vec{\alpha}(\vec{k})\cdot\vec{\sigma} - t_{+}F(\vec{k})\mathbb{1}, \tag{4}$$

where $\mathbb{1}$ is the identity matrix and $\vec{\alpha} = (\alpha_x(\vec{k}), -\alpha_y(\vec{k}), \alpha_z(\vec{k}))$ with its components given by

$$\alpha_x(\vec{k}) = [1 + \cos(\theta_s + \vec{k}\cdot\vec{a}_1) + \cos(\theta_s - \vec{k}\cdot\vec{a}_2)]t_0 + \{\cos[(\vec{a}_1 + \vec{a}_2)\cdot\vec{k}] + 2\cos[\theta_s + (\vec{a}_1 - \vec{a}_2)\cdot\vec{k}]\}t_2, \tag{5a}$$

$$\alpha_y(\vec{k}) = [\sin(\theta_s + \vec{k}\cdot\vec{a}_1) - \sin(\theta_s - \vec{k}\cdot\vec{a}_2)]t_0 + \sin[(\vec{a}_1 + \vec{a}_2)\cdot\vec{k}]t_2, \quad \text{and} \quad \alpha_z(\vec{k}) = \delta - t_{-}F(\vec{k}). \tag{5b}$$

Since $H_{\mathrm{mex}}$ does not explicitly depend on time and $[\vec{\alpha}\cdot\vec{\sigma}, -t_{+}F(\vec{k})\mathbb{1}] = 0$, the time-evolution operator for the Hamiltonian defined in Eq. (4) is given by

$$e^{-\frac{i}{\hbar}H_{\mathrm{mex}}\Delta t} = e^{-i\vec{\beta}\cdot\vec{\sigma}} e^{-\frac{i}{\hbar}[-t_{+}F(\vec{k})\mathbb{1}]\Delta t}, \tag{6}$$

where $\vec{\beta} = \vec{\alpha}\Delta t/\hbar$.

From the well-known properties of the Pauli matrices, the first exponential on the right-hand side of Eq. (6) yields

$$e^{-i\vec{\beta}\cdot\vec{\sigma}} = \cos(\beta)\mathbb{1} - \frac{i\sin(\beta)}{\beta}\begin{pmatrix} \beta_z & \beta_x - i\beta_y \\ \beta_x + i\beta_y & \beta_z \end{pmatrix} = \mathcal{M}, \tag{7}$$

where $\beta = |\vec{\beta}|$, and the second exponential of Eq. (6) is equivalent to

$$e^{\frac{i}{\hbar}[t_{+}F(\vec{k})\mathbb{1}\Delta t]} = \mathbb{1}e^{\frac{i}{\hbar}[t_{+}F(\vec{k})\Delta t]} = \mathcal{N}. \tag{8}$$

Applying the time-evolution operator defined in Eq. (6) on the wave function $\Psi(\vec{r}, t)$, one obtains the propagated wave function after a time step $\Delta t$ as

$$\Psi(\vec{r}, t + \Delta t) = e^{-\frac{i}{\hbar}H_{\mathrm{mex}}\Delta t}\Psi(\vec{r}, t) = \mathcal{M}\mathcal{N}\Psi(\vec{r}, t). \tag{9}$$

Note that $\mathcal{M}$ and $\mathcal{N}$ depend on the wave vector $\vec{k}$, therefore, the matrix multiplication with a general initial wave packet is conveniently computed numerically in reciprocal space by performing a Fourier transform on the wave function, which gives this method a flavor of a semianalytical procedure. At $t = 0$, we assume the wave function as a circularly symmetric 2D Gaussian wave packet with width $d$ multiplied by the pseudospinor $[C_1 C_2]^T$, such as

$$\Psi(\vec{r}, t) = N\begin{pmatrix} C_1 \\ C_2 \end{pmatrix}\exp\left[-\frac{(x - x_0)^2 - (y - y_0)^2}{d^2}\right], \tag{10}$$

where $N$ is the normalization factor and $(x_0, y_0)$ are the coordinates of the center of the Gaussian wave packet in real space. As the exciton is normally excited by a low-momentum photon, we assume a moiré exciton exactly at the Γ point of the moiré Brillouin zone, i.e., with zero energy and zero momentum.

*Wave packet dynamics and Zitterbewegung.*—Figure 2 illustrates the average position $\langle x(t)\rangle$ and $\langle y(t)\rangle$ of the wave packet as a function of time for $d = 200$ Å (blue), 300 Å (orange), and $d = 500$ Å (green). Different pseudospin polarizations $[C_1\, C_2]^T = [0\,1]^T$ and $[1\,1]^T$ are considered, with and without an applied electric field $\varepsilon$, as indicated on top of each panel. Results for $[1\, i]^T$ are given in the

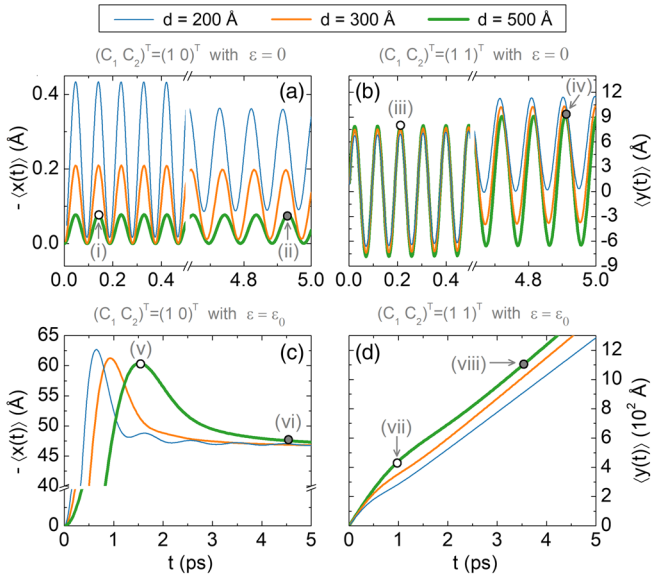


FIG. 2. ZBW of the expectation values of the position of a moiré exciton in a $MoS_2/WSe_2$ vdWHS, considering an initial Gaussian wave packet distribution with $d = 200$ Å (blue), $d = 300$ Å (orange), and $d = 500$ Å (green), and pseudospinors $[C_1\,C_2]^T = [1\,0]^T$ and $[C_1\,C_2]^T = [1\,1]^T$, under applied fields (a),(b) $\varepsilon = 0$ and (c),(d) $\varepsilon = \varepsilon_0$. The propagated probability densities for the time instants marked with white and gray circular dots in each panel are shown in Fig. 3.

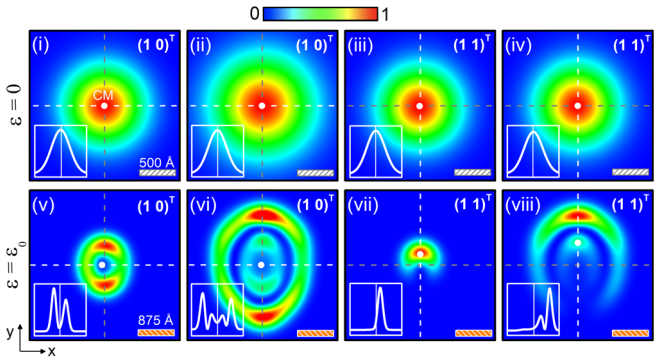


FIG. 3. Snapshots of the propagated probability density $|\Psi(\vec{r},t)|^2$ for an initial Gaussian wave packet with width $d = 500$ Å and pseudospinors $[1\,0]^T$ and $[11]^T$. Top (bottom) row shows results for applied electric field $\varepsilon = 0$ ($\varepsilon = \varepsilon_0$). The white (orange) bar corresponds to 500 Å (875 Å) and the small white dot inside each panel represents the center of mass of the wave packet. The profiles of $|\Psi(\vec{r},t)|^2$ along the dashed white lines in each panel are shown as insets. The labels (i)–(viii) correspond to different time steps as marked with circular dots in Fig. 2.

Supplemental Material [36], along with the material parameters for the vdWHSs studied here. The pseudospinor represents the occupation of the $A$ and $B$ sublattice sites; therefore, it is expected to be controlled in an actual experiment by the polarization of the excitation light, since the $R_h^h$ and $R_h^X$ regions, which correspond to the $A$ and $B$ sublattices here, exhibit different selection rules for circular light polarization [38]. For instance, a circular light polarization that excites ILEs only in $R_h^h$ ($R_h^X$) regions would effectively produces a moiré exciton wave packet with pseudospinor $[C_1\,C_2]^T = [1\,0]^T$ ($[0\,1]^T$). As for the wave packet width, it could be controlled, e.g., by the focus of the short-pulse excitation light, although actual precise manipulation and engineering of excitonic wave packets may be a challenging task [39]. Laser spots as narrow as ≈500 Å, i.e., of the same order of magnitude as the wave packets considered here, have been used for the study of exciton dynamics in 2D semiconductors in recent experiments [40–43].

In the absence of an external applied electric field ($\varepsilon = 0$), both expectation values $\langle x(t)\rangle$ and $\langle y(t)\rangle$ exhibit ZBW, but with very low amplitude and high frequency, which hinders the actual observation of this effect. On the other hand, for $\varepsilon = \varepsilon_0$, where the gap is closed and moiré exciton effectively behaves as a massless Dirac quasiparticle, the wave packet moves only in one direction, exhibiting damped oscillations. For conciseness, Figs. 2(c) and 2(d) show only the moving component of $\vec{r}$, see the Supplemental Material for the other component [36]. In this case, the amplitude of the oscillation is much higher, of the order of tens of angstroms, with a timescale on the order of few picoseconds, which would make this effect clearly observable in actual experiments. Wave packets with smaller width exhibit weak oscillations, which vanish as the width increases. Nevertheless, for a $[1\,0]^T$ spinor wave packet, a ≈60 Å peak, followed by a ≈50 Å permanent shift of the center of the wave packet, is observed for all values of wave packet width considered here. For larger widths, the motion resembles the one of zero-energy electron wave packets in monolayer graphene [44,45], since the wave packet becomes narrower around the Γ point of the moiré Brillouin zone, where dispersion is approximately the same as in graphene. The dependence of the maximum displacement of the expectation value $\langle x(t)\rangle$ as a function of $\epsilon$, as well as the time for this maximum displacement to occur, is discussed in the Supplemental Material [36], where it is demonstrated that both the maximum wave packet displacement and its timescale are highest at $\varepsilon = \varepsilon_0$.

As for a $[1\,1]^T$ spinor wave packet, the center of mass is predicted to move almost linearly with time, traveling tens of angstroms in just a few picoseconds, before the exciton recombines.

The unique features predicted here for the moiré exciton wave packet dynamics can also be observed in the probability density distribution, as shown in Fig. 3. An initial Gaussian wave packet for the center-of-mass coordinate of a free exciton is expected to simply disperse across space as time elapses. Similar dispersion is observed, e.g., in Refs. [40,42] for monolayer TMDs. Notice, however, that the Gaussian packet in those experiments represented a density distribution of multiple excitons, rather than an actual single exciton wave function,

so that phonon effects [46], which give rise to a halo in the exciton distribution, play an important role. In our case, in order to avoid such phonon hot spots [46] and exciton-exciton interaction effects, one would have to employ low-intensity exciting irradiation at low temperatures, so that the exciton distribution effectively matches the noninteracting excitons picture proposed here. In this case, the moiré exciton wave packet evolves as a double ring structure in the presence of an electric field with the critical value $\varepsilon_0$, whereas the usual dispersion is observed in the absence of field. The observation of this strikingly different wave packet dispersion in time in the presence of the applied field would thus represent a smoking gun evidence of the ZBW of moiré excitons and their Dirac-like nature.

*Conclusion.*—In summary, we argue that dynamics of a moiré exciton wave packet is an advantageous solid-state optoelectronic platform to probe ZBW, evasive in experiments to date. In $MoS_2/WSe_2$ vdWHSs with small twist angles, the moiré pattern created by the interlayer lattice mismatch produces a periodic in plane potential for the ILE center-of-mass and, consequently, a moiré exciton band structure. A moiré exciton wave packet in this system exhibits very fast and weak oscillations, hard to detect experimentally. However, in the presence of a perpendicular electric field, the gap of the moiré exciton band structure can be closed, which attributes the characteristics of a massless Dirac fermion to this quasiparticle, so ZBW becomes naturally more evident. In such a case, we reveal a shift of tens of angstroms in the center of the moiré exciton wave packet, along with damped oscillations with picosecond long periods. The exciton probability density profile is demonstrated to be strikingly different in the presence of gap-closing electric field, compared to the case without any field. The density profile and motion is also shown to be strongly dependent on the pseudospinor of the moiré exciton wave packet, which is controllable by the polarization of the incident exciting light. With relevant timescales being within reach of available experimental techniques, we expect to instigate the first experimental detection of ZBW in an exciton wave packet, which opens the gate to follow-up studies exploiting thereby proven massless Dirac fermion character of the moiré excitons in $MoS_2/WSe_2$ vdWHSs induced by gating.

This work was supported by the Brazilian Council for Research (CNPq), through the PRONEX/FUNCAP, Universal, and PQ programs, the Brazilian National Council for the Improvement of Higher Education (CAPES), and the Research Foundation—Flanders (FWO).

[1] P. A. M. Dirac, Proc. R. Soc. A **117**, 610 (1928).
[2] E. Schrödinger, Sitz. Preuss. Akad. Wiss. Phys.-Math. Kl. **24**, 418 (1930).
[3] W. Greiner *et al.*, *Relativistic Quantum Mechanics* (Springer, Berlin, 2000), Vol. 2.
[4] K. Huang, Am. J. Phys. **20**, 479 (1952).
[5] T. M. Rusin and W. Zawadzki, Phys. Rev. B **80**, 045416 (2009).
[6] J. Y. Vaishnav and C. W. Clark, Phys. Rev. Lett. **100**, 153002 (2008).
[7] M. Merkl, F. E. Zimmer, G. Juzeliūnas, and P. öhberg, Europhys. Lett. **83**, 54002 (2008).
[8] J. Schliemann, D. Loss, and R. M. Westervelt, Phys. Rev. Lett. **94**, 206801 (2005).
[9] W. Zawadzki, Phys. Rev. B **72**, 085217 (2005).
[10] J. Schliemann, D. Loss, and R. M. Westervelt, Phys. Rev. B **73**, 085323 (2006).
[11] T. M. Rusin and W. Zawadzki, J. Phys. Condens. Matter **19**, 136219 (2007).
[12] J. Schliemann, Phys. Rev. B **77**, 125303 (2008).
[13] T. Biswas and T. K. Ghosh, J. Appl. Phys. **115**, 213701 (2014).
[14] W. Zawadzki, Phys. Rev. B **74**, 205439 (2006).
[15] L. K. Shi, S. C. Zhang, and K. Chang, Phys. Rev. B **87**, 161115(R) (2013).
[16] L. Ferrari and G. Russo, Phys. Rev. B **42**, 7454 (1990).
[17] W. Zawadzki and T. M. Rusin, Phys. Lett. A **374**, 3533 (2010).
[18] F. Cannata and L. Ferrari, Phys. Rev. B **44**, 8599 (1991).
[19] S. V. Vonsovskii, M. S. Svirskii, and L. M. Svirskaya, Theor. Math. Phys. **94**, 243 (1993).
[20] L. Lamata, J. León, T. Schätz, and E. Solano, Phys. Rev. Lett. **98**, 253005 (2007).
[21] S. M. Cunha, D. R. da Costa, G. O. de Sousa, A. Chaves, J. M. Pereira, and G. A. Farias, Phys. Rev. B **99**, 235424 (2019).
[22] Y.-X. Wang, Z. Yang, and S.-J. Xiong, Europhys. Lett. **89**, 17007 (2010).
[23] R. Gerritsma, G. Kirchmair, F. Zähringer, E. Solano, R. Blatt, and C. F. Roos, Nature (London) **463**, 68 (2010).
[24] L. J. LeBlanc, M. C. Beeler, K. Jiménez-García, A. R. Perry, S. Sugawa, R. A. Williams, and I. B. Spielman, New J. Phys. **15**, 073011 (2013).
[25] C. Qu, C. Hamner, M. Gong, C. Zhang, and P. Engels, Phys. Rev. A **88**, 021604(R) (2013).
[26] T. L. Silva, E. R. F. Taillebois, R. M. Gomes, S. P. Walborn, and A. T. Avelar, Phys. Rev. A **99**, 022332 (2019).
[27] M.-Y. Li, C.-H. Chen, Y. Shi, and L.-J. Li, Mater. Today **19**, 322 (2016).
[28] Y. Liu, N. O. Weiss, X. Duan, H.-C. Cheng, Y. Huang, and X. Duan, Nat. Rev. Mater. **1**, 1 (2016).
[29] C. Zhang, C.-P. Chuu, X. Ren, M.-Y. Li, L.-J. Li, C. Jin, M.-Y. Chou, and C.-K. Shih, Sci. Adv. **3**, e1601459 (2017).
[30] L. Zhang, Z. Zhang, F. Wu, D. Wang, R. Gogna, S. Hou, K. Watanabe, T. Taniguchi, K. Kulkarni, T. Kuo *et al.*, Nat. Commun. **11**, 5888 (2020).
[31] H. Yu, G.-B. Liu, J. Tang, X. Xu, and W. Yao, Sci. Adv. **3**, e1701696 (2017).
[32] A. Chaves, G. A. Farias, F. M. Peeters, and R. Ferreira, Commun. Comput. Phys. **17**, 850 (2015).
[33] D. R. da Costa, A. Chaves, S. H. R. Sena, G. A. Farias, and F. M. Peeters, Phys. Rev. B **92**, 045417 (2015).
[34] Y. Wang, Z. Wang, W. Yao, G.-B. Liu, and H. Yu, Phys. Rev. B **95**, 115429 (2017).
[35] J. Ibanez-Azpiroz, A. Eiguren, A. Bergara, G. Pettini, and M. Modugno, Phys. Rev. A **87**, 011602(R) (2013).

[36] See Supplemental Material at http://link.aps.org/supplemental/10.1103/PhysRevLett.127.106801 for material parameters, hopping energies, and complementary results on the wave packet dynamics assuming different pseudospinors.
[37] S. M. Cunha, D. R. da Costa, G. O. de Sousa, A. Chaves, J. M. Pereira, Jr., and G. A. Farias, Phys. Rev. B **99**, 235424 (2019).
[38] K. Tran *et al.*, Nature **567**, 71 (2019).
[39] X. Zang, S. Montangero, L. D. Carr, and M. T. Lusk, Phys. Rev. B **95**, 195423 (2017).
[40] J. Zipfel, M. Kulig, R. Perea-Causín, S. Brem, J. D. Ziegler, R. Rosati, T. Taniguchi, K. Watanabe, M. M. Glazov, E. Malic *et al.*, Phys. Rev. B **101**, 115430 (2020).
[41] R. Perea-Causin, S. Brem, R. Rosati, R. Jago, M. Kulig, J. D. Ziegler, J. Zipfel, A. Chernikov, and E. Malic, Nano Lett. **19**, 7317 (2019).
[42] M. Kulig, J. Zipfel, P. Nagler, S. Blanter, C. Schüller, T. Korn, N. Paradiso, M. M. Glazov, and A. Chernikov, Phys. Rev. Lett. **120**, 207401 (2018).
[43] D. Unuchek, A. Ciarrocchi, A. Avsar, Z. Sun, K. Watanabe, T. Taniguchi, and A. Kis, Nat. Nanotechnol. **14**, 1104 (2019).
[44] I. R. Lavor, D. R. da Costa, A. Chaves, S. Sena, G. Farias, B. Van Duppen, and F. M. Peeters, J. Phys. Condens. Matter **33**, 095503 (2021).
[45] G. M. Maksimova, V. Y. Demikhovskii, and E. V. Frolova, Phys. Rev. B **78**, 235321 (2008).
[46] M. M. Glazov, Phys. Rev. B **100**, 045426 (2019).